Structural Basis for the Preference of UTP over ATP in Human Deoxycytidine Kinase: Illuminating the Role of Main-Chain Reorganization†

Michael H. Godsey,‡ Stephan Ort,§ Elisabetta Sabini,‡ Manfred Konrad,§ and Arnon Lavie*,‡

Department of Biochemistry and Molecular Genetics, University of Illinois at Chicago, 900 South Ashland Avenue, Chicago, Illinois 60607, and Department of Molecular Genetics, Max Planck Institute for Biophysical Chemistry, Am Fassberg 11, D-37077 Göttingen, Germany

Received September 13, 2005; Revised Manuscript Received November 1, 2005

ABSTRACT: Human deoxycytidine kinase (dCK) uses nucleoside triphosphates to phosphorylate several clinically important prodrugs in addition to its natural substrates. Although UTP is the preferred phosphoryl donor for this reaction, our previous studies reported dCK structures solely containing ADP in the phosphoryl donor binding site. To determine the molecular basis of the kinetically observed phosphoryl donor preference, we solved crystal structures of a dCK variant lacking a flexible insert (residues 65−79) but having similar catalytic properties as wild type, in complex with deoxycytidine (dC) and UDP, and in the presence of dC but the absence of UDP or ADP. These structures reveal major changes in the donor base binding loop (residues 240−247) between the UDP-bound and ADP-bound forms, involving significant main-chain rearrangement. This loop is disordered in the dCK-dC structure, which lacks a ligand at the phosphoryl donor site. In comparison with the ADP-bound form, in the presence of UDP this loop is shifted inward to make closer contact to the smaller uracil base. These structures illuminate the phosphoryl donor binding and preference mechanisms of dCK.

In its physiological role in the nucleoside salvage pathway, deoxycytidine kinase (EC 2.7.1.74) phosphorylates deoxycytidine (dC),[1] deoxyguanosine (dG), and deoxyadenosine (dA) to their monophosphate forms using nucleoside triphosphates as phosphoryl donors. Additional enzymes of the salvage pathway subsequently convert these nucleoside monophosphates to their triphosphate forms. In addition to being an essential enzyme for phosphorylation of natural substrates, dCK has garnered attention as the first and rate-limiting enzyme in the activation of many clinically important prodrugs. Nucleoside analogues (NAs) known to be substrates of dCK include the antineoplastic agents cladribine (2-chloro-2′-deoxyadenosine) (*1*) and AraC (1-*β*-D-arabinofuranosylcytosine) (*2*) and the antiviral compounds ddC (2′,3′-dideoxycytidine) (*3*) and 3TC (2′-deoxy-3′-thiacytidine) (*4*). Highlighting the pivotal role of dCK for the activation of NAs is the fact that resistance to nucleoside analogues is linked to loss of dCK activity (*5*−*7*), and increasing intracellular levels of dCK restore sensitivity to or enhance the toxicity of nucleoside analogues (*8*, *9*). Human dCK is a very slow enzyme, with a turnover rate well below 1 s^{-1} (*10*), which is appreciably slower than some other deoxynucleoside kinases including dGK and dNK (*11*, *12*), suggesting that dCK has potential to be made much more active toward both natural substrates and nucleoside prodrugs using protein engineering techniques. Indeed, some progress has been made in this area (*13*). These and other findings highlight the role of dCK as an important target of study in relation to current and future NA prodrug therapies, in both cancer and antiviral applications.

While ATP is thought to be the common phosphoryl donor for kinase reactions in the cell, an early study showed that dCK is capable of using numerous nucleoside triphosphates (*14*), and following studies determined that dCK is able to use most of the endogenous nucleoside triphosphates as donor molecules (*15*, *16*). Remarkably, a recent report finds that even inorganic triphosphate is able to serve as a phosphoryl donor for dCK (*17*) albeit with a 10-fold larger K_m than ATP. Further studies indicated that UTP, rather than ATP, is the physiological phosphoryl donor for dCK (*18*, *19*), and several groups have probed the kinetic behavior of dCK with UTP (*10*, *20*). Reported K_m values for UTP are near 1 μM, while reported K_m values for ATP range from 7 to 54 μM (*10*, *18*, *21*), and the k_{cat}/K_m ratios favor UTP over ATP by up to a factor of 50 (*10*). In addition to being more active with UTP, dCK is also more resistant to dCTP inhibition when using UTP, such that the normal in vivo level of 10−20 μM dCTP (*22*) is unlikely to have a significant effect on dCK activity in the presence of UTP (*19*, *20*). Although the usual ratio of ATP to UTP in cells is approximately 2:1 (*22*, *23*), these kinetic analyses demonstrate that UTP is likely to be the preferred phosphoryl donor in vivo.

† M.H.G., A.L., and E.S. were supported by NIH Grant CA095687, with additional funding for M.H.G. by NIH Training Grant HL07692. S.O. and M.K. were supported by the Deutsche Forschungsgemeinschaft and the Max Planck Society.

* Address correspondence to this author. Tel: 312-355-5029. Fax: 312-355-4535. E-mail: lavie@uic.edu.

‡ University of Illinois at Chicago.

§ Max Planck Institute for Biophysical Chemistry.

[1] Abbreviations: dCK, deoxycytidine kinase; dCKΔI, dCK lacking residues 65−79; dGK, deoxyguanosine kinase; dNK, deoxynucleoside kinase; UTP, uridine triphosphate; UDP, uridine diphosphate; ATP, adenosine triphosphate; ADP, adenosine diphosphate; dC, deoxycytidine; dA, deoxyadenosine; dG, deoxyguanosine; NTP, nucleoside triphosphate; NA, nucleoside analogue; WT, wild type.

10.1021/bi0518646 CCC: $33.50
Published on Web 12/06/2005

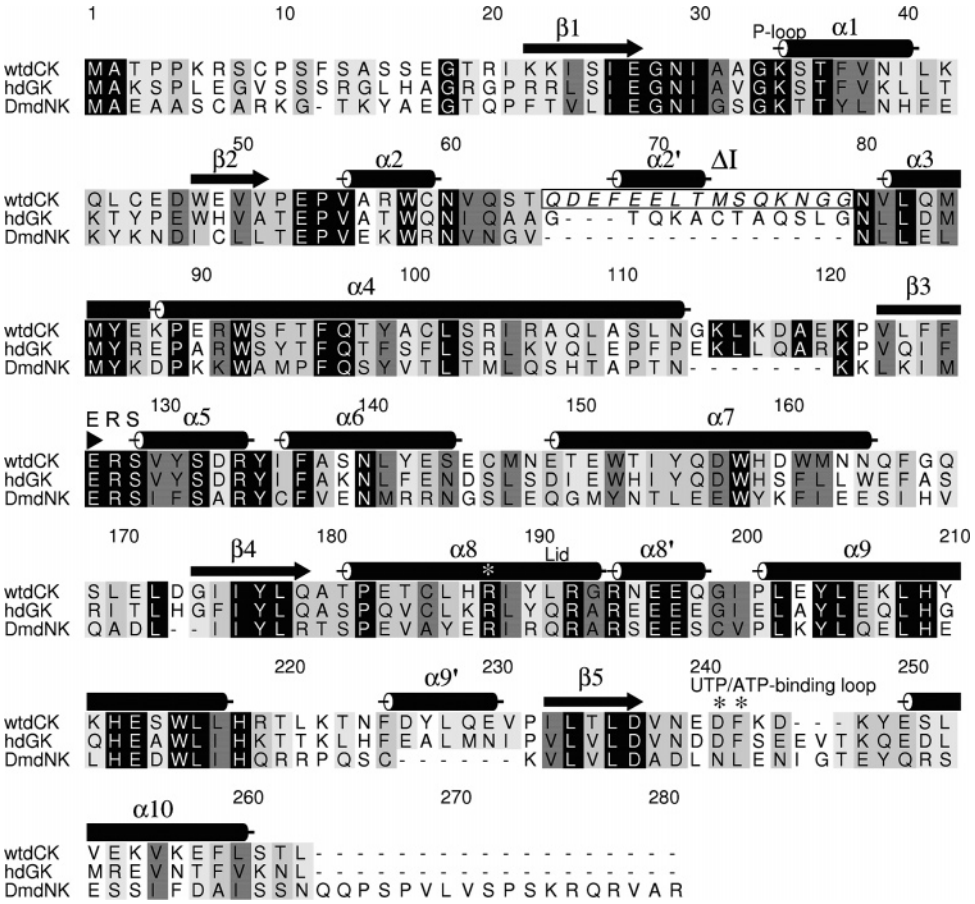

FIGURE 1: Sequence alignment of human dCK, human dGK, and dNK from *D. melanogaster*. Numbering is from the wild-type dCK sequence. Secondary structural elements and locations of conserved motifs are shown above the sequences. Residues which directly interact with the uracil base of UDP are labeled with asterisks. The residues which are deleted in dCKΔI are boxed and shown in italics.

Despite the role of UTP as primary phosphoryl donor, available crystal structures of dCK contain ADP in the phosphoryl donor binding site, which emulates ATP binding. The structure of dCK was first solved in complexes with ADP and one of three pyrimidine phosphoryl acceptors (dC, AraC, and gemcitabine), representing "dead-end" complexes of substrate and product (*13*). Based upon the structures of other kinases, such as thymidylate kinase (*24*), ADP is expected to bind in the same location and manner as ATP or ATP analogues. While illuminating ATP binding of dCK, these structures did not directly suggest a mechanism of UTP base recognition and binding. To address this issue, we attempted to cocrystallize full-length dCK in complex with UDP but were unsuccessful in obtaining crystals. However, a dCK construct lacking a flexible insert (residue 65−79), yet showing nucleoside kinase activities very similar to the full-length protein, did form suitable crystals. In the study presented here using this construct (dCKΔI), UDP is found in a similar position as was observed for ADP. Unexpectedly, significant main-chain rearrangement takes place to accommodate the smaller uracil base. The herein described conformational change could not have been predicted from the previously available structures of dCK, nor those of human deoxyguanosine kinase (dGK) and *Drosophila melanogaster* deoxynucleoside kinase (dNK) (*25*, *26*). These proteins are homologous to dCK (48% and 30% identity, respectively) (Figure 1), and alignments of the three structures show considerable similarity (Cα rms deviation of 1.1 Å for each using 177 atoms for dNK and 206 atoms for dGK). They vary from dCK in activity and substrate specificity, although there is overlap in their substrate sets. The dNK is able to phosphorylate all four natural deoxynucleosides at a similar rate, though K_m values vary by up to 3 orders of magnitude using ATP as phosphoryl donor (*11*). Like human dCK, dGK from *Bacillus subtilis* has been shown to be much more effective with UTP than ATP (*27*). The structure of human dGK unexpectedly contained the phosphoryl donor ATP in the acceptor binding site, while dNK was solved with dTTP, dThy, or dC in the acceptor binding site (*25*, *26*). Moreover, the dNK structure lacks the phosphoryl-donor base-binding loop and its following helix (as predicted by sequence alignment with dCK and dGK). Since these structures lack ligands within the phosphoryl donor site, they are of little help in understanding phosphoryl donor binding and preference.

We studied the binding of both adenine and uridine phosphoryl donors to dCK because of the importance of dCK in NA prodrug metabolism, its role in chemotherapy, the potential of exploiting this knowledge for catalytic improvement, and the preference of this kinase for an unusual phosphoryl donor. By characterizing the ability of dCK to use alternative triphosphates, we might be able to optimize the enzyme at this site to use phosphoryl donors of our choosing, which could prove helpful in future therapeutic applications. To advance our understanding of NTP discrimination by dCK, we solved the structures of human dCK in two new complexes: the binary dCK−dC complex, and the ternary dCK−dC−UDP complex. Comparison with the

ADP-bound complexes (*13*) shows that the phosphates of UDP and ADP as well as the uracil and adenine bases assume similar positions and orientations. However, a short loop (residues 240−247) before the C-terminal α-helix is shifted significantly between the ADP- and UDP-bound forms while this loop is disordered in the binary dCK−dC complex.

EXPERIMENTAL PROCEDURES

Mutant Design and Construction. A new human dCK form (dCKΔI) was constructed that lacks an insert region (residues 65−79) based upon a structural alignment with the *D. melanogaster* dNK. This construct was originally designed to probe the function of the insert region but, in addition, fortuitously formed diffraction quality crystals in complex with UDP. The dCKΔI loop deletion was constructed using the PCR fusion method. As in the wild-type dCK structures (*13*), an N-terminal three-residue (GSH) sequence is present in dCKΔI after thrombin cleavage of the N-terminal histidine tag. For simplicity of comparison to the ADP structures, the sequence numbering used in this report corresponds to the wild-type residue numbers, rather than the numerical sequence found in dCKΔI; i.e., Thr64 is followed directly by Asn80.

Protein Expression, Purification, and Crystallization. The insert deletion mutant dCKΔI was grown as previously described for wild-type dCK (*13*). *Escherichia coli* carrying the recombinant plasmid were grown at 37 °C in 2YT media, induced with 0.1 mM IPTG, and harvested after 4 h. Cells were lysed by sonication and clarified by ultracentrifugation (1 h, 40000 rpm), and the supernatant containing the protein was loaded onto a TALON Superflow Co^{2+} affinity column (Clontech). After the column was washed overnight with 1 L of buffer containing 50 mM Tris-HCl, pH 7.5, 300 mM KCl, and 10% glycerol, 100 units of thrombin was loaded onto the column and recirculated overnight to cleave the 6×His tag. The cut protein was eluted with buffer, concentrated, and further purified on an S-200 gel filtration column (Amersham). Protein was found to be >95% pure by Coomassie-stained SDS−PAGE. Complexes were formed by dialysis of the protein in a buffer solution containing dC or dC and UDP. The final protein solutions for crystallization contained 10 mg/mL protein, 4 mM ligand(s), 25 mM Tris-HCl, pH 7.5, 50 mM KCl, 4 mM $MgCl_2$, and 2 mM DTT. Nucleosides, nucleotides, and other chemicals were purchased from Sigma. Crystals were grown by the hanging drop vapor diffusion method. The crystallization solution contained 13−14% PEG 1000, 9% 2-methyl-2,4-pentanediol (MPD), 200 mM $CaCl_2$, and 100 mM sodium cacodylate, pH 6.5. Protein and crystallization solutions were mixed 1:1 in the hanging drop. Crystals typically grew in 1−3 days at 22 °C as diamond-shaped layered plates to dimensions of approximately 300 × 200 × 20 μm.

Data Collection and Processing. Crystals required no additional cryoprotection for freezing in liquid nitrogen. X-ray diffraction data were collected at 100 K at the Advanced Photon Source using the SERCAT beamline BM-22 at $\lambda = 0.97626$ Å using a MAR165 CCD detector. Data were collected for both crystals to 3 Å. The crystals belong to space group $P2_1$ (dCK/dC) or $P2_12_12_1$ (dCK/dC/UDP), with solvent contents of 48.1% and 47.8%, respectively, both corresponding to four monomers per asymmetric unit. Data were indexed, scaled, and merged using XDS and XSCALE (*28*). Data collection and refinement statistics are shown in Table 1.

Table 1: Data Collection and Refinement Statistics

	dC only	dC/UDP
Data Collection		
wavelength (Å)	0.976	0.976
temperature (K)	100	100
resolution (Å)	3.0	3.0
reflections		
observed	62424	125036
unique	18725	21704
completeness (%)[a]	83.7 (53.4)	96.3 (91.2)
R_{sym} (%)[a,b]	11.8 (54.2)	11.8 (41.0)
$I/\sigma(I)$[a]	8.8 (2.4)	12.6 (3.5)
redundancy	3.3 (1.9)	5.7 (5.3)
Crystal Attributes		
space group	$P2_1$	$P2_12_12_1$
unit cell		
a (Å)	79.34	64.20
b (Å)	64.94	110.89
c (Å)	108.60	155.40
β (deg)	96.0	
molecules/ASU	4	4
Refinement		
R_{cryst} (%)[c]	23.5	24.6
R_{free} (%)[d]	28.5	30.0
resolution range (Å)	20−3.0	30−3.0
no. of atoms		
protein	6852	7169
dC	16 × 4	16 × 4
UDP		25 × 4
waters	26	55
rms deviation		
bond length (Å)	0.009	0.009
bond angles (deg)	1.2	1.3
average *B* factor (Å^2)		
protein	70.1	44.9
main chain	71.3	45.3
side chain	68.7	44.5
dC	51.6	31.6
UDP		49.7
waters	46.2	23.3

[a] Highest resolution shell in parentheses. [b] $R_{sym} = \sum_{hkl}|I_{hkl} - \langle I_{hkl}\rangle|/\sum_{hkl}\langle I_{hkl}\rangle$. [c] $R_{cryst} = \sum_{hkl}|F_o(hkl) - F_c(hkl)|/\sum_{hkl}|F_o(hkl)|$. [d] $R_{free} = R_{cryst}$, calculated for 10% randomly selected reflections not included in refinement.

Structure Determination and Refinement. The structures were solved by molecular replacement using the program AMoRe (*29*) with the previously reported dCK dimer (PDB ID 1P60) as a search model. After rigid-body refinement, an initial electron density map was calculated. Density was clearly visible for ligands and the turn created at the insert-deletion site. Noncrystallographic symmetry restraints covering most of the model were used during refinement. Cycles of model building and refinement were performed in O (*30*) and CNS (*31*), respectively. Some surface loops in some of the molecules were not visible. Water molecules were added manually. Evaluation of the structures was performed with PROCHECK (*32*). Coordinates and structure factors have been deposited with the Protein Data Bank (accession codes 2A2Z for the dCKΔI/dC/UDP complex and 2A30 for the dCKΔI/dC complex).

Steady-State Kinetic Assays. Spectrophotometric assays (*13*, *33*) were performed in 50 mM Tris-HCl, pH 7.5, 100 mM KCl, and 5 mM $MgCl_2$ at 37 °C. dCK or dCKΔI was present at 0.4 μM in all experiments. For phosphoryl acceptor

Table 2: Kinetic Analysis of dCKΔI and Wild-Type Human dCK Using Constant Donor Concentrations[a]

substituent		WT ATP (1000 μM)	ΔI ATP (1000 μM)	WT UTP (1000 μM)	ΔI UTP (1000 μM)
dC	k_{cat}	0.033 ± 0.001	0.049 ± 0.004	0.044 ± 0.001	0.088 ± 0.007
	K_m	<1	1.4 ± 0.5	<1	<1
	k_{cat}/K_m	>33 × 10^3	36 × 10^3	>44 × 10^3	>88 × 10^3
dA	k_{cat}	1.7 ± 0.1	2.8 ± 0.2	0.33 ± 0.02	0.31 ± 0.02
	K_m	100 ± 20	415 ± 60	13 ± 3	53 ± 10
	k_{cat}/K_m	17 × 10^3	6.7 × 10^3	25 × 10^3	5.9 × 10^3
dG	k_{cat}	2.6 ± 0.1	2.2 ± 0.1	0.33 ± 0.02	0.32 ± 0.01
	K_m	231 ± 20	474 ± 30	21 ± 4	87 ± 10
	k_{cat}/K_m	11 × 10^3	4.6 × 10^3	16 × 10^3	3.7 × 10^3
AraC	k_{cat}	0.30 ± 0.02	0.41 ± 0.04	0.17 ± 0.02	0.15 ± 0.02
	K_m	6.9 ± 2	13 ± 3	2.7 ± 1	2.8 ± 1
	k_{cat}/K_m	43 × 10^3	32 × 10^3	63 × 10^3	54 × 10^3

[a] Values shown are the averages of at least two experiments. k_{cat} are in s^{-1}, K_m are in μM, and k_{cat}/K_m are in M^{-1} s^{-1}, and standard deviations are shown.

Table 3: Kinetic Analysis of dCKΔI and Wild-Type Human dCK Using Constant Acceptor Concentrations[a]

substituent		WT dC (100 μM)	ΔI dC (100 μM)	WT AraC (250 μM)	ΔI AraC (250 μM)
ATP	k_{cat}	0.028 ± 0.001	0.039 ± 0.001	0.40 ± 0.02	0.36 ± 0.01
	K_m	3.5 ± 0.4	2.9 ± 0.3	93 ± 10	53 ± 3
	k_{cat}/K_m	8.0 × 10^3	13 × 10^3	4.3 × 10^3	6.8 × 10^3
UTP	k_{cat}	0.031 ± 0.002	0.041 ± 0.001	0.093 ± 0.003	0.075 ± 0.002
	K_m	2.3 ± 0.4	1.5 ± 0.2	10 ± 1.0	4.7 ± 0.4
	k_{cat}/K_m	14 × 10^3	27 × 10^3	9.3 × 10^3	16 × 10^3

[a] Values shown are the averages of at least two experiments. k_{cat} are in s^{-1}, K_m are in μM, and k_{cat}/K_m are in M^{-1} s^{-1}, and standard deviations are shown.

measurements, ATP·Mg or UTP·Mg was kept constant at 1 mM, while acceptor concentrations were varied between 1 and 700 μM, depending upon the substrate being tested (Table 2). For phosphoryl donor measurements, dC was 100 μM, or AraC was 250 μM, while donor concentrations varied from 1 to 500 μM (Table 3). Sensitivity of this optical assay is limited using concentrations below ~5 μM for acceptor molecules and ~1 μM for donors (a lower limit for the donors is due to their regeneration by the auxiliary enzymes). At the lowest substrate concentrations, this assay deviates from ideal Michaelis−Menten kinetics due to the relatively low ratio of substrate to enzyme. However, because of the slow rate of catalysis by dCK, applying a lower enzyme concentration proved impractical. All experiments were performed in duplicate or greater. Data were fit to the Michaelis−Menten equation using SigmaPlot.

RESULTS

We have solved the structures of human deoxycytidine kinase in complexes with dC at the acceptor site, and with dC and UDP, the product of the true phosphoryl donor, UTP, to 3 Å resolution. Because the previously solved crystal form of human wild-type deoxycytidine kinase would not grow to diffraction quality except in the presence of ADP (*13*), alternative enzymatically active constructs were produced and subjected to crystal screening in the presence of various substrates, products, and inhibitors. One dCK construct (dCKΔI) lacking a flexible insert (residues 65−79) of unknown function was able to crystallize with dC in the acceptor site and with, or without, nucleotide at the phosphoryl donor site. The design of this deletion construct was based upon the prediction that the lack of this insert would not perturb the overall structure. This prediction was based upon the fact that (i) such an insert is missing in dNK, (ii) no electron density was visible for this insert in the dGK structure, and (iii) no electron density for this insert was seen in the dCK structures except for one monomer of the orthorhombic space group, where it was stabilized by a crystal contact to a symmetry-related molecule. Prior to this work, the function of this insert was unknown, besides a few references to amino acid differences of this insert in the human and murine enzyme (*34*). However, in a recent study, no significant kinetic effects were observed due to limited mutations in the insert region (*35*). Here we reveal a possible function of this insert by kinetic comparison of dCKΔI to the full-length wild-type enzyme (see below).

Unfortunately, the dCKΔI crystals grow in layered plates, and only two complexes have proven sufficiently amenable to optimization to produce data quality crystals. These crystals were formed from the binary dCK−dC and the ternary dCK−dC−UDP complexes. Only small (~50 μm per side) plate-type crystals would grow before layering of plates. These were used in collection of X-ray diffraction data, and the structures of these two dCK complexes were solved by molecular replacement. Although the two crystals appeared visually similar and grew from the same crystallization conditions, somewhat unexpectedly, they have different space groups with related cell edges. The binary complex grew in the space group $P2_1$ with cell dimensions of $a_2 = 79.4$ Å, $b_2 = 64.9$ Å, $c_2 = 108.6$ Å, and $\beta = 96.0°$, while the ternary complex was $P2_12_12_1$ with cell dimensions of $a_3 = 64.2$ Å, $b_3 = 110.9$ Å, and $c_3 = 155.4$ Å. After the structures were solved, it became clear that the dimers in the asymmetric units of the two crystal forms were spatially related; i.e., by overlaying one dimer from the binary complex onto a related dimer from the ternary complex, the alternate dimers from both complexes occupy the nearly same space. The major difference between the alternate dimers is their orientation, which is only slightly shifted between the two, but apparently to such an extent to change the space

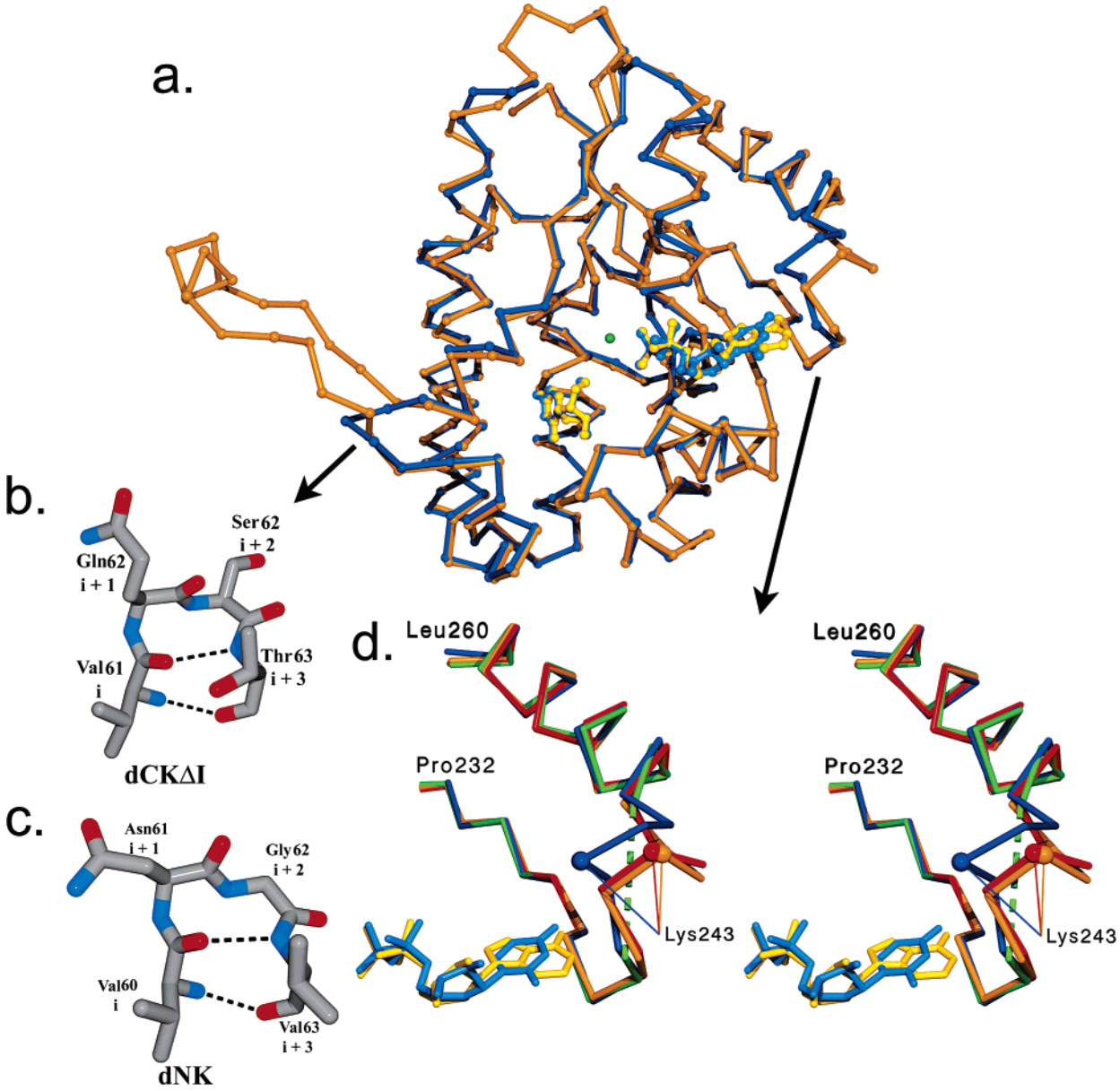

FIGURE 2: (a) α-carbon traces of dCKΔI bound to dC and UDP (blue) and of dCK wild type bound to dC and ADP (gold; PDB ID 1P60, molecule A). The catalytic Mg^{2+} ion is shown in green. (b, c) Comparison of the type I′ β-turns found in dCKΔI and dNK from *D. melanogaster*. (d) Stereoview of Cα traces in the region of donor base binding. Shown are dCKΔI bound to dC/UDP in blue (PDB ID 2A2Z), dC only in green (PDB ID 2A30), and dC/ADP (PDB IDs 1P60 in gold and 1P61 in red). The Cα positions of Lys243 are shown to highlight the difference in main-chain conformations. A green dashed line represents the disordered residues in the dC-only structure.

group. It therefore seems possible that the layering of plates observed in the crystals was due to a mixture of these two closely related crystal growth patterns, and only by using small, single-layered crystals were we able to find one space group or the other.

Overall Structure. Human dCK is a 260-residue protein with a molecular mass of 30.5 kDa. The construct used in our studies, dCKΔI, lacks an insert of 15 residues (residues 65−79) and has a molecular mass of 28.8 kDa. For ease of comparison, residue numbering in this construct will retain the wild-type protein numbering system. The structures were built beginning at residue 20 and extend through to the C-terminus. In the structure with dC alone the phosphoryl-donor base-binding loop (residues 240−247) showed no clear electron density and was not modeled. Some of the surface loops are poorly ordered in both crystal forms, as evidenced by poor density and high *B* factors in refinement. In all structures, dCKΔI, like wild-type dCK, is a homodimeric globular protein consisting of a five-stranded parallel β-sheet surrounded by 10 α-helices. The overall structures in both the binary and ternary complexes are identical to the previously reported structures of dCK (*13*) throughout most parts of the protein (rms deviations between 221 Cα atoms of 0.55−0.60 Å) (Figure 2a). Except for the presence or absence of UDP and the disorder of the phosphoryl-donor base-binding loop, the binary and ternary complexes are essentially identical. For this reason and for simplicity, the majority of this report will be referring to the ternary complex, unless specifically stated otherwise. The three conserved nucleoside kinase motifs (the P-loop, ERS motif, and LID region) are also similar to those seen in the ADP structures. The binding of dC is effectively identical in all of the dCK and dCKΔI structures and will not be described here. A four-helix bundle (helices α4 and α7 from each

monomer) forms the dimer interface. For a complete treatment of these features and overall structure, refer to Sabini et al. (*13*). As in the previous dCK structures, molecular topology and dimerization are similar to those seen in the structures of dGK and dNK.

Structure and Function of the Insert Region. The missing insert region (residues 65−79) is replaced by a type I′ β-turn in our structures, consisting of residues $V_{61}QST_{64}$ (Figure 2b,c). Normally, this type of turn requires a glycine in the $i + 2$ position for steric reasons. This position is occupied by Ser63 in this case, causing some variation from the standard type I′ geometry. The ϕ and ψ angles are 58° and 45° for Gln62 and 58° and 35° for Ser63 (placing both residues in the allowed region of Ramachandran space), while in a model example of a type I′ β-turn these values are 60° and 30° for $i + 1$ and 90° and 0° for $i + 2$. Because of the deleted residues, Thr64 and Asn80 are sequential. Residues Cys59 and Asn80 are unmoved from their positions in the wild-type structures. In addition to removing a disordered region, this new β-turn appears to have allowed the formation of a Ca^{2+}-mediated crystal contact between the Oδ of Asn60 and the backbone oxygen of Glu230. Interestingly, dNK also makes a type I′ β-turn here, with residues $V_{60}NGV_{63}$, before reacquiring structural similarity to wild-type dCK and dGK. The Asn and Gly of positions $i + 1$ and $i + 2$ in dNK are more typical of this type of turn than the Gln and Ser found in our construct. Accordingly, these mutations have been made to our dCK construct, and their effects on kinetics and crystallization are being tested. A similar internal loop modification approach was shown to improve crystallization of the AHL synthetase LasI from *Pseudomonas aeruginosa* (*36*, *37*).

To explore the effects of the loss of this insert region upon activity, kinetic studies were undertaken with dCK and dCKΔI using the natural substrates of dCK (dA, dG, and dC) and the nucleoside analogue AraC, with either ATP or UTP as phosphoryl donors (Tables 2 and 3). In most cases, the k_{cat} values measured with dCKΔI were very similar to those measured with wild-type dCK. In fact, under some acceptor/donor combinations, the dCKΔI exhibited slightly increased k_{cat} over wild type. However, significant differences were seen for the K_m values of purine nucleoside acceptors between the wild-type and ΔI enzyme (Table 2). In contrast, the K_m values for pyrimidine nucleoside acceptor were only slightly increased by the absence of the insert. Thus, it seems that the insert plays a role in the purine/pyrimidine selectivity at the acceptor site. From the structure, we cannot directly derive a mechanism of how the insert exerts its influence on the acceptor, except that the insert is located between helices α2 and α3, which contain residues that contact the acceptor nucleoside.

Kinetic Characterization of dCK WT and dCKΔI with UTP and ATP. As has been reported elsewhere (*18*−*20*), the K_m values for acceptors are lower when using UTP compared to using ATP as phosphoryl donor. For example, the decrease in the K_m of dA upon the switch to UTP is 7-fold in both the wild-type dCK and dCKΔI proteins (Table 2). This UTP-mediated effect for dG was a 12-fold reduction in K_m with wild-type dCK and a 6-fold reduction in K_m with dCKΔI. However, concomitant decreases are seen in the k_{cat} values when using UTP instead of ATP as the phosphoryl donor, largely offsetting the K_m decreases. The result of this is similar enzymatic efficiencies (k_{cat}/K_m values) for the purine nucleosides regardless of whether UTP or ATP is used as the phosphoryl donor. This is true for both wild-type dCK and dCKΔI. In contrast to the purine substrates, the k_{cat} values of the pyrimidines dC and AraC show smaller dependence upon the choice of phosphoryl donor. In the wild-type enzyme, the k_{cat} of dC is nearly identical with ATP and UTP, and that of AraC is only slightly smaller using UTP instead of ATP.

The kinetic constants of the phosphoryl donors ATP or UTP were measured with either dC or AraC as acceptors (Table 3). When using dC as acceptor nucleoside, we observed small or insignificant differences in the K_m and k_{cat} values of UTP versus ATP with both the wild-type dCK and the dCKΔI derivative. In contrast, with AraC as acceptor, in both wild-type dCK and dCKΔI proteins, the k_{cat} values measured with UTP were 4−5-fold smaller, yet the K_m values were approximately 10-fold smaller than those measured with ATP, leading to overall increases in the enzymatic efficiencies with UTP over ATP. The K_m values for either phosphoryl donor observed in dCKΔI were approximately one-half of those for the wild-type enzyme, while the corresponding k_{cat} values were similar, leading to small advantages in enzymatic efficiency for dCKΔI over dCK. In summary, using AraC as a phosphoryl acceptor, dCKΔI performed similarly to wild-type dCK with regard to its preference for UTP over ATP, with both enzymes favoring UTP approximately 2-fold.

The finding of dCK and dCKΔI behaving similarly to each other with the two phosphoryl donors (but do show differences with respect to the acceptor; see below) suggests that the insert region is not highly involved in binding of the phosphoryl donor or release of the diphosphate product. This result gives confidence that the atomic details of UDP binding observed in our structures of dCKΔI are unaffected by the absence of this insert.

Comparison of the dC/UDP and dC/ADP Structures. In the area of the P-loop (residues 28−35), UDP binding by dCKΔI is similar to ADP binding. The phosphates and P-loop residues overlay within error between the dCK structures containing the catalytic Mg^{2+} ion. In the ADP-bound structure lacking this ion (PDB ID 1P60), the side chains of Ser35 and Glu127 are turned away from their Mg^{2+}-coordinated positions. In both the UDP- and ADP-bound structures, two oxygen atoms of the β-phosphate are coordinated by backbone amines of residues 31, 33, and 34 and by the Nζ of Lys34, while the other oxygen coordinates the catalytic Mg^{2+} and the side chains of Ser35 and Glu127, which are also coordinating the Mg^{2+}. The α-phosphates contact the backbone amines of residues 34 and 35 and the side-chain NH of Arg192. In the binary dCKΔI/dC structure, the side chain of Lys34 is shifted, or has become disordered, and some waters are observed to compensate for the absence of phosphates, but otherwise the structure of the phosphate-binding region remains generally unchanged from the ADP- or UDP-bound forms.

Similar to what was observed in the ADP-bound structures, there are no apparent close contacts between the sugar moiety of UDP and the enzyme. The rings of the sugars appear to be suspended between the phosphates and the base, which are better anchored to the protein. The UDP ribosyl ring is approximately 4 Å away from the backbone of residues 188,

191, and 192 on one side and about 4.5 Å from Thr36 on the other. Because of the limited resolution of the dCKΔI/dC/UDP structure, it is difficult to precisely determine the pucker of this sugar though it has been modeled in the C2′-endo form because it fits into the density slightly better than other forms. This is the same sugar pucker seen in the ADP complex structures.

The functionally and structurally significant differences between the UDP-bound structure and ADP-bound structures occur in a flexible loop between β5 and α10 (residues 240−247). This loop contacts the adenine or uracil base and is the primary base-recognition element. The backbone and several side chains are involved in the recognition of the uracil base (Figure 3). The carboxylic oxygen of Asp241 makes a hydrogen bond to N3, and an additional H-bond is made from O4 to the backbone amide of Phe242 (the omit density for residues Asp241, Phe242, and the bound UDP is presented in Supporting Information). The O2, the other potential hydrogen bond acceptor, is left exposed to solvent. At 3 Å resolution, no water molecule is readily visible near this atom. On the other side of the uracil base, the phenyl group of Phe242 packs with its face roughly perpendicular to the C4−C5 edge. This inward shift of the phenyl group, compared to the ADP-bound structures, seems to pull this loop toward the core of the protein by several angstroms, especially between residues 242 and 246. Similar to observations in the ADP-bound structures, the base is stacked atop the extended side chain of Arg188, which is held in place by hydrogen bonds to backbone oxygens of Ala32, Val238, and Asn239.

Compared with uracil recognition, binding of adenosine involves different contacts to the amino acids at the 241 and 242 positions. While the uracil base interacts with the side chains of Asp241 and Phe242, the adenine base makes hydrogen bonds only to backbone atoms in this loop, specifically between N6 and the backbone carbonyl of Glu240 and between N1 and the backbone amide of Phe242. The phenyl group of Phe242 is flipped away from the base (relative to the UDP-bound form). Even though UDP makes a hydrogen bond to the same atom, because of the larger size of the adenine base when ADP hydrogen bonds to the backbone at Phe242, the remainder of the loop is pushed slightly further away from the body of the protein (∼1−3 Å). This loop (residues 241−246) is disordered in the dCK−dC binary complex crystal structure, in which the NTP phosphoryl donor binding site is unoccupied. This indicates that the structure of this region is flexible until a specific conformation is formed upon binding of ligand, the choice of which is dependent upon phosphoryl donor identity. The structural differences in this loop are significant enough to disrupt a crystal contact that was found in this region in the ADP-bound structures, explaining why dCK crystals would not grow with UDP in those crystal forms. This region is not involved in crystal contacts in the dCKΔI/dC and dCKΔI/dC/UDP complexes.

DISCUSSION

Nucleoside kinases are critical in supplying nucleotide precursors for DNA synthesis through the phosphorylation of nucleosides into their monophosphate forms. Interest in structural and functional features of dCK is high due to its importance in phosphorylating several clinically used nucleoside analogues, including the pyrimidines AraC and gemcitabine and the purines fludarabine and cladribine. In addition to the substrate promiscuity of dCK at the acceptor site, this enzyme accepts several triphosphates as phosphoryl donors. That dCK can utilize nucleoside triphosphates other than ATP is not surprising. In fact, most nucleoside and nucleoside monophosphate kinases can accept several nucleoside triphosphates as substrates (*27*). However, in most of these cases, ATP is assumed to be the preferred phosphoryl donor in the cellular environment. What makes dCK unusual is that UTP, even when considering the higher in vivo concentration of ATP, seems to be the physiological phosphoryl donor (*10*, *18*−*20*). To understand the preference of dCK for UTP over ATP, we solved the crystal structure of dCKΔI in the presence of UDP and compared it to the available structures of dCK solved in the presence of ADP. To our knowledge, this is the first structure of a nucleoside kinase or nucleoside monophosphate kinase where a non-adenine-containing nucleotide is observed in the phosphoryl donor site.

Not surprisingly, UDP and ADP are found to bind at the same site. Residues that bind the phosphates of these nucleotides differ only slightly in their positions, and the sugar moiety does not make direct interactions to the protein in either case. However, the loop (residues 240−247) that interacts directly with the base moiety of the donors adopts different main-chain conformations depending upon if UDP or ADP is bound. In fact, we do not observe electron density for this loop in the absence of a donor molecule (see below). Because of the similarity in phosphate binding modes and lack of sugar contacts, it appears that phosphoryl donor discrimination resides primarily, if not solely, in this loop. Thus, to utilize either the purine ATP or the pyrimidine UTP at the phosphoryl donor site, significant main-chain rearrangement must occur.

Of particular importance are Asp241 and Phe242 to donor nucleotide binding, being accomplished via side-chain interactions in the case of UDP and via backbone interactions in the case of ADP. Such a homologous loop is also present in other nucleoside kinases. These two residues are conserved in dGK (dGK Asp255 and Phe256), although the dGK loop contains an additional three residues. Interestingly, this loop is visible in the dGK structure lacking a ligand in the donor site, albeit with some of the highest *B* factors in the model (*25*), in contrast to our experience with dCK, where it is disordered when this site is empty. On the other hand, the absence of density in the reported *Drosophila* dNK structure, also lacking a ligand in this site, is consistent with our observation (*26*). The above-mentioned Asp/Phe pair is not strictly conserved in dNK, and on the basis of structural and sequence alignments, it is likely that residues with similar chemical properties (the Asn209/Leu210 pair) occupy these positions in dNK.

As stated previously, kinetic analysis of dCK-catalyzed phosphorylation using several triphosphates revealed a lower K_m value for UTP versus ATP, prompting the conclusion that UTP is the physiological phosphoryl donor used by dCK (*10*). In our experiments we also observe this preference for UTP. However, since when using dC as the acceptor nucleoside our measured K_m value for ATP (3.5 μM) is only slightly higher than that of UTP (2.3 μM), the preference for UTP is less significant. Note that with AraC as acceptor

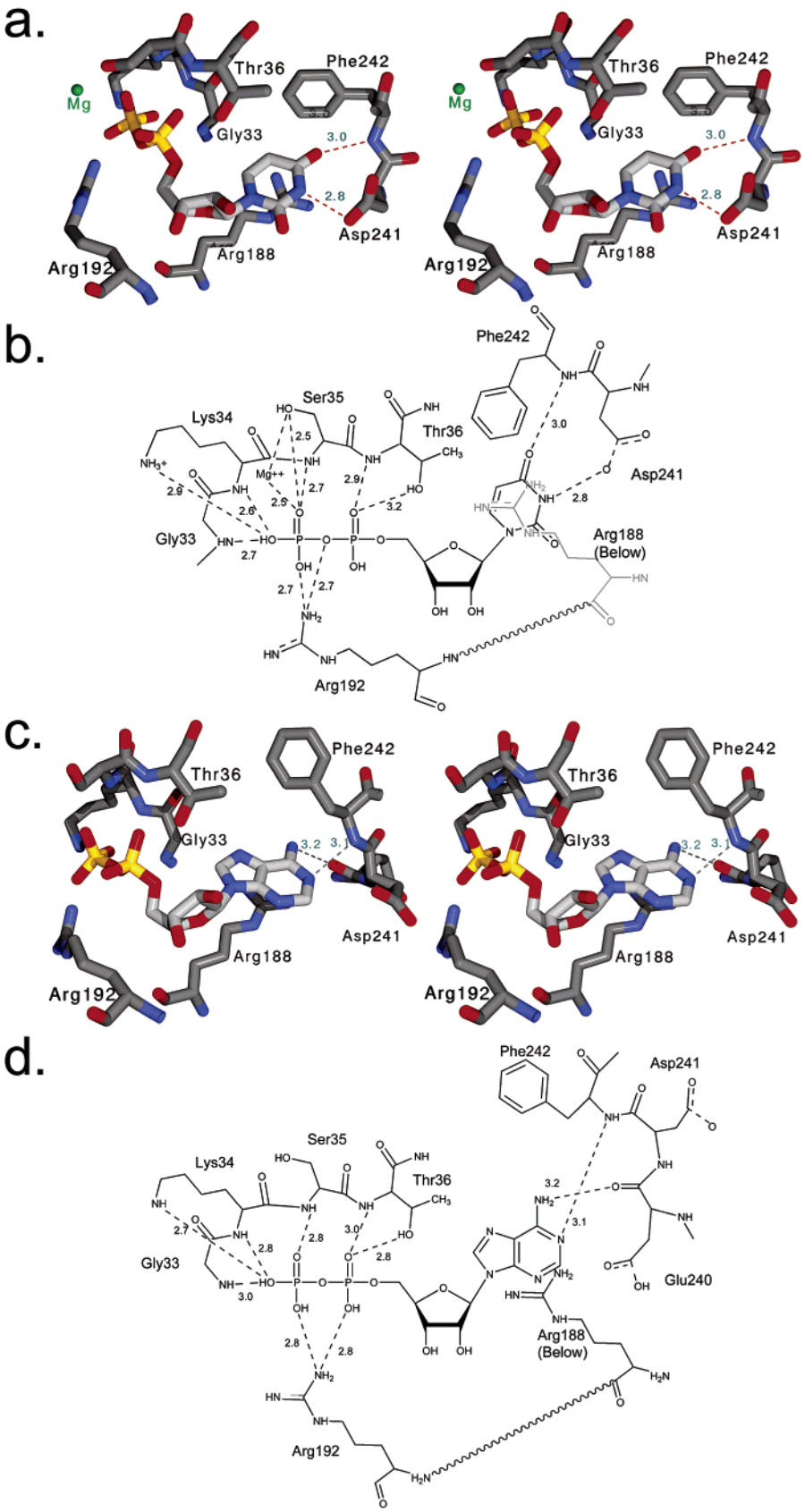

FIGURE 3: (a) Stereo image of UDP binding by dCKΔI. (b) Schematic representation of UDP binding by dCKΔI. (c) Stereo image of ADP binding by dCK as seen in 1P60, molecule A. (d) Schematic representation of ADP binding by dCK as seen in 1P60, molecule A. Significant main-chain and side-chain conformational changes occur in residues that directly contact the base moieties of the nucleotides, residues 240−242. At the same time, there is similarity between the UDP- and ADP-bound forms in phosphate binding and lack of contact to the sugar moieties.

we do observe a much-reduced K_m for UTP (10 μM) versus ATP (93 μM), consistent with the conclusion that UTP is the preferred physiological phosphoryl donor. Inspection of the literature reveals that the K_m for ATP in human dCK

measured with dC ranges from 54 to 7 μM. Further analysis reveals that experiments conducted with enzyme from cell lines, or from leukemic patients, exhibit a higher ATP K_m value [54 μM (*10*); 30 μM (*38*); 20 μM (*18*); 15 μM (*20*)] in comparison to data obtained using recombinant dCK [7 μM (*21*); 3.5 μM, this study]. Thus, the relatively low K_m value we measure for ATP could be due to our use of recombinantly produced enzyme, suggesting some kind of posttranslational modification or other regulatory mechanism that is present in dCK purified from human cells. In fact, in vitro phosphorylation of dCK by protein kinase Cα has been reported (*39*), and more recently, it was shown that phosphatase treatment affects the activity of dCK purified from lymphocytes but has no effect on recombinant dCK (*40*). Surprisingly, the K_m values for UTP measured either with cell-purified dCK or with recombinant dCK do not show this variation and cluster within a narrow range between 0.8 and 2.3 μM (this report and refs *10*, *18*, and *20*). Since the UDP-bound dCK and the ADP-bound dCK have a different conformation in the phosphoryl-donor base-binding loop, it is conceivable that a posttranslational phosphorylation could influence one but not the other conformation.

Inspection of the kinetic parameters listed in Tables 2 and 3 reveals a consistent direct relationship between K_m and k_{cat} values: high K_m correlate with high k_{cat}. This is true both for the nucleoside acceptor site and for the nucleotide donor site. As an example for this relationship at the acceptor site we refer to the nucleoside dG: its K_m is larger with ATP as the donor nucleotide (231 μM) than with UTP (21 μM), but concomitantly, the k_{cat} with ATP (2.6 s^{-1}) is larger than that measured with UTP (0.33 s^{-1}). Likewise, the K_m value of ATP is larger than that of UTP when measured with AraC (93 versus 10 μM), but the k_{cat} is also higher with ATP over that with UTP (0.4 versus 0.093 s^{-1}). Thus, the nature of acceptor nucleoside affects the K_m values of the donor nucleotide, and vice versa. In either case, a lowering of the K_m results in a lowered k_{cat}. However, we do note that, in all of the cases we examined, a decrease in K_m by a certain factor results in a reduced k_{cat} by a smaller factor. As a consequence, the lowering of the acceptor K_m by UTP in comparison to ATP (Table 2), which albeit also lowers the k_{cat} but by a smaller factor, yields an overall increase in k_{cat}/K_m for UTP over ATP.

It is not clear how UTP decreases the nucleoside acceptor K_m values in comparison to ATP (i.e., the allosteric effect of the phosphoryl donor on the nucleoside) nor why the K_m of UTP is lower than that of ATP. Keeping in mind that the K_m values must not directly correlate to K_d values and lacking crystal structures of dCK in complex with ATP or UTP (see below), we analyzed our ADP and UDP structures to gain an understanding for the lower UTP K_m value over that of ATP. In both structures the number (but not the specific atoms involved) of hydrogen bonds between the base of the phosphoryl donor and the enzyme is the same. The most notable difference is in the position of the side chain of Phe242. In the dC−UDP complex, due to the main-chain rearrangement of the phosphoryl-donor base-binding loop, this side chain is buried in a hydrophobic environment formed by Phe37, Val238, and Tyr246. In contrast, in the dC−ADP structure, this phenyl side chain swings outward leaving a cavity that is occupied by two water molecules. Therefore, the dC−UDP conformation could be preferred over the dC−ADP conformation for both entropic (release of the two water molecules) and enthalpic (increased hydrophobic interactions) reasons.

UTP and ATP are not the only triphosphates utilized by dCK. In fact, Hughes et al. found that dTTP and GTP are better phosphoryl donors than ATP but worse than UTP in the dC kinase reaction (*10*). Modeling dTTP binding to dCK based on the UDP structure reveals a close contact (~2.4 Å) between the thymine methyl group and the side chain of Phe242. As a consequence, a slight readjustment of the phenyl group is predicted to occur in the presence of dTTP. Otherwise, the interactions with the thymine base are predicted to be very similar to those observed with a uridine base. In the case of GTP acting as the phosphoryl donor, inspection of the two conformations of the 241−247 loop suggests that GTP would fit better when the enzyme adopts the conformation as seen with ADP. However, due to the different hydrogen-bonding patterns between adenine and guanine, a rotation of the guanine base by ~20° in comparison to the adenine base will be required to position the base in a productive position for hydrogen bond interactions. In this model of GTP binding to dCK, the guanine O6 atom hydrogen bonds with the main-chain NH group of Phe242, the N1 atom with the carbonyl of Glu240, and the amino group at position 2 with the side chain of Asp241. Thus, different to the situation of ATP binding where only main-chain interactions are made with the adenine base, our model predicts that for GTP, beyond to two such main-chain interactions, an additional side-chain interaction with Asp241 will take place, as observed in the UDP structure. However, given the demonstrated flexibility of the 241−247 loop, we cannot rule out that an as yet unseen conformation will be adopted upon GTP binding. Given this flexibility, it is not surprising that CTP can also act as a phosphoryl donor, albeit with a 10-fold reduced efficiency compared to UTP (*10*). In contrast, probably due to the acceptor site being optimized for dC binding, the K_m value for dC being about 50-fold lower than that for cytidine, dCTP does not function as a phosphoryl donor and is in fact a feedback inhibitor of the dCK-catalyzed reaction (*38*).

In addition to dCK having a lower K_m for UTP versus ATP, UTP has large effects upon the kinetic constants of the acceptor nucleosides. We found for both wild-type dCK and the dCKΔI variant that using UTP as a phosphoryl donor significantly lowered the K_m values for purine acceptors and AraC, albeit with an associated decrease in k_{cat}, as had been seen before (*10*, *18*, *20*, *34*, *35*). In previous studies of human dCK the reported K_m values for dC with UTP are 2−5-fold lower than those found with ATP (*10*, *20*, *34*). A similar differential effect of NTPs has also been seen in other nucleoside kinases, for example, the dGK from *B. subtilis*, where the K_m for dG was 0.6 μM with UTP but 6.5 μM with ATP (*27*). It is hard to rationalize the lower K_m values of nucleoside acceptors in the presence of UTP over ATP based solely on structural comparisons between the dC−ADP and dC−UDP structures since the dC and its surrounding residues appear in similar positions in the two structures. The γ-phosphates of ATP or UTP, which are absent in our diphosphate nucleotides, may differ in their positions in such a way as to alter the acceptor binding pocket and therefore change the affinity of the protein for acceptors. Alternatively, it is conceivable that the effect on acceptor K_m is due to the more global difference in donor binding by altering the reaction mechanism, for example, by changing from a

random bi-bi with ATP to a sequential mechanism that prefers UTP binding prior to dC, as was suggested previously by both steady-state (*10*) and transient kinetic studies (*41*).

In addition to supplying a molecular rationale for the acceptance of UTP by dCK, our studies shed light on the function of the 15-residue insert located between helices 2 and 3. Our prediction that deletion of this insert would not abolish activity was substantiated by the nearly wild-type activity of the dCKΔI construct used here. However, steady-state kinetic experiments with this construct reveal that this insert plays a role in increasing the affinity for purine nucleosides at the acceptor site (Table 2). Such an interpretation is consistent with the fact that thymidine kinase 2, which is predicted to be structurally similar to dCK and dGK (*13*, *25*), does not contain such an insert and does not phosphorylate purines, whereas dGK, which phosphorylates dG and dA, does. Also, in the *D. melanogaster* sole nucleoside kinase, dNK, which lacks such an insert, the K_m values of the pyrimidines are lower than those of the purines. We speculate that the insert functions to lower the K_m values for purines by affecting the conformational flexibility of its flanking α-helices. Since these helices contribute to the nucleoside binding site, it is expected that they change conformation upon acceptor binding.

Lastly, since dCK is of primary importance in the activation of nucleoside analogue prodrugs, we aim not only at understanding its structural and kinetic features but also at improving its activity toward these compounds. On the basis of the information obtained in this study, one potential approach to increasing the activity of dCK is to modify the donor recognition loop, particularly at residues Asp241 and Phe242.

ACKNOWLEDGMENT

We thank the staff at SERCAT for assistance in data collection. Data were collected at Southeast Regional Collaborative Access Team (SER-CAT) 22-BM beamline at the Advanced Photon Source, Argonne National Laboratory. Supporting institutions may be found at www.ser-cat.org/members.html. Use of the Advanced Photon Source was supported by the U.S. Department of Energy, Office of Science, Office of Basic Energy Sciences, under Contract W-31-109-Eng-38.

SUPPORTING INFORMATION AVAILABLE

One figure showing omit density for residues Asp241, Phe242, and the bound UDP. This material is available free of charge via the Internet at http://pubs.acs.org.

REFERENCES

1. Spasokoukotskaja, T., Arner, E. S., Brosjo, O., Gunven, P., Juliusson, G., Liliemark, J., and Eriksson, S. (1995) *Eur. J. Cancer 31A*, 202−208.
2. Kierdaszuk, B., Krawiec, K., Kazimierczuk, Z., Jacobsson, U., Johansson, N. G., Munch-Petersen, B., Eriksson, S., and Shugar, D. (1998) *Adv. Exp. Med. Biol. 431*, 623−627.
3. Johnson, M. A., Johns, D. G., and Fridland, A. (1987) *Biochem. Biophys. Res. Commun. 148*, 1252−1258.
4. Kewn, S., Veal, G. J., Hoggard, P. G., Barry, M. G., and Back, D. J. (1997) *Biochem. Pharmacol. 54*, 589−595.
5. Stegmann, A. P., Honders, M. W., Hagemeijer, A., Hoebee, B., Willemze, R., and Landegent, J. E. (1995) *Ann. Hematol. 71*, 41−47.
6. Mansson, E., Spasokoukotskaja, T., Sallstrom, J., Eriksson, S., and Albertioni, F. (1999) *Cancer Res. 59*, 5956−5963.
7. Groschel, B., Himmel, N., Cinatl, J., Perigaud, C., Gosselin, G., Imbach, J. L., Doerr, H. W., and Cinatl, J., Jr. (1999) *Nucleosides Nucleotides 18*, 921−926.
8. Hapke, D. M., Stegmann, A. P., and Mitchell, B. S. (1996) *Cancer Res. 56*, 2343−2347.
9. Stegmann, A. P., Honders, W. H., Willemze, R., Ruiz van Haperen, V. W., and Landegent, J. E. (1995) *Blood 85*, 1188−1194.
10. Hughes, T. L., Hahn, T. M., Reynolds, K. K., and Shewach, D. S. (1997) *Biochemistry 36*, 7540−7547.
11. Johansson, M., van Rompay, A. R., Degreve, B., Balzarini, J., and Karlsson, A. (1999) *J. Biol. Chem. 274*, 23814−23819.
12. Yamada, Y., Goto, H., and Ogasawara, N. (1982) *Biochim. Biophys. Acta 709*, 265−272.
13. Sabini, E., Ort, S., Monnerjahn, C., Konrad, M., and Lavie, A. (2003) *Nat. Struct. Biol. 10*, 513−519.
14. Durham, J. P., and Ives, D. H. (1970) *J. Biol. Chem. 245*, 2276−2284.
15. Datta, N. S., Shewach, D. S., Hurley, M. C., Mitchell, B. S., and Fox, I. H. (1989) *Biochemistry 28*, 114−123.
16. Sarup, J. C., Johnson, M. A., Verhoef, V., and Fridland, A. (1989) *Biochem. Pharmacol. 38*, 2601−2607.
17. Krawiec, K., Kierdaszuk, B., and Shugar, D. (2003) *Biochem. Biophys. Res. Commun. 301*, 192−197.
18. White, J. C., and Capizzi, R. L. (1991) *Cancer Res. 51*, 2559−2565.
19. Shewach, D. S., Reynolds, K. K., and Hertel, L. (1992) *Mol. Pharmacol. 42*, 518−524.
20. Krawiec, K., Kierdaszuk, B., Eriksson, S., Munch-Petersen, B., and Shugar, D. (1995) *Biochem. Biophys. Res. Commun. 216*, 42−48.
21. Krawiec, K., Kierdaszuk, B., Kalinichenko, E. N., Rubinova, E. B., Mikhailopulo, I. A., Eriksson, S., Munch-Petersen, B., and Shugar, D. (2003) *Nucleosides, Nucleotides, Nucleic Acids 22*, 153−173.
22. Traut, T. W. (1994) *Mol. Cell. Biochem. 140*, 1−22.
23. Hauschka, P. V. (1973) *Methods Cell Biol. 7*, 361−462.
24. Ostermann, N., Schlichting, I., Brundiers, R., Konrad, M., Reinstein, J., Veit, T., Goody, R. S., and Lavie, A. (2000) *Struct. Folding Des. 8*, 629−642.
25. Johansson, K., Ramaswamy, S., Ljungcrantz, C., Knecht, W., Piskur, J., Munch-Petersen, B., Eriksson, S., and Eklund, H. (2001) *Nat. Struct. Biol. 8*, 616−620.
26. Mikkelsen, N. E., Johansson, K., Karlsson, A., Knecht, W., Andersen, G., Piskur, J., Munch-Petersen, B., and Eklund, H. (2003) *Biochemistry 42*, 5706−5712.
27. Andersen, R. B., and Neuhard, J. (2001) *J. Biol. Chem. 276*, 5518−5524.
28. Kabsch, W. (1993) *J. Appl. Crystallogr. 24*, 795−800.
29. Navaza, J. (1994) *Acta Crystallogr. A50*, 157−163.
30. Jones, T. A., Zou, J. Y., Cowan, S. W., and Kjeldgaard. (1991) *Acta Crystallogr. A47*, 110−119.
31. Brünger, A. T., Adams, P. D., Clore, G. M., Delano, W. L., Gros, P., Grosse-Kunstleve, R. W., Jiang, J.-S., Kuszewskli, J., Nilges, N., Read, R. J., Rice, L. M., Simonson, T., and Warren, G. L. (1998) *Acta Crystallogr. D54*, 905−921.
32. Laskowski, R. A., MacArthur, M. W., Moss, D. S., and Thornton, J. M. (1993) *J. Appl. Crystallogr. 26*, 283−291.
33. Agarwal, K. C., Miech, R. P., and Parks, R. E., Jr. (1978) *Methods Enzymol. 51*, 483−490.
34. Johansson, M., and Karlsson, A. (1995) *Biochem. Pharmacol. 50*, 163−168.
35. Usova, E. V., and Eriksson, S. (2002) *Biochem. Pharmacol. 64*, 1559−1567.
36. Gould, T. A., Watson, W. T., Choi, K. H., Schweizer, H. P., and Churchill, M. E. (2004) *Acta Crystallogr. D60*, 518−520 (Epub 2004 Feb 25).
37. Gould, T. A., Schweizer, H. P., and Churchill, M. E. (2004) *Mol. Microbiol. 53*, 1135−1146.
38. Kim, M. Y., and Ives, D. H. (1989) *Biochemistry 28*, 9043−9047.
39. Wang, L. M., and Kucera, G. L. (1994) *Biochim. Biophys. Acta 1224*, 161−167.
40. Csapo, Z., Sasvari-Szekely, M., Spasokoukotskaja, T., Talianidis, I., Eriksson, S., and Staub, M. (2001) *Biochem. Pharmacol. 61*, 191−197.
41. Turk, B., Awad, R., Usova, E. V., Bjork, I., and Eriksson, S. (1999) *Biochemistry 38*, 8555−8561.

BI0518646